Oxygen isotope heterogeneity of the mantle beneath the Canary Islands: insights from olivine phenocrysts

Andrey A. Gurenko [a]*, Ilya N. Bindeman [b], Marc Chaussidon [a]

[a] Centre de Recherches Pétrographiques et Géochimiques, CNRS-INSU-Nancy Université, BP 20, F-54501 Vandoeuvre-lès-Nancy, France

[b] Department of Geological Sciences, 1272 University of Oregon, Eugene, OR 97403, USA

Revised version,

submitted to *Contributions to Mineralogy and Petrology,*

November 16, 2010

Components:

Abstract: 413 words; 2,758 characters with spaces;

Main text: 6,969 words; 45,030 characters with spaces;

7 figures, 1 table; list of references includes 68 citations.

On-line Supplementary Information: 1 table and 1 figure composed of 5 phototables

*** Corresponding author and present address:**

Andrey Gurenko, Centre de Recherches Pétrographiqueset Géochimiques, 15, rue Notre-Dame des Pauvres, B.P. 20, 54501 Vandoeuvre-lès-Nancy, France. Phone: +33 (0)3 83 59 48 75, Fax: +33 (0)3 83 51 17 98, E-mail: agurenko@crpg.cnrs-nancy.fr

Abstract

A relatively narrow range of oxygen isotopic ratios ($\delta^{18}O$ = 5.0–5.4‰) is preserved in olivine of mantle xenoliths, mid-ocean ridge (MORB) and most ocean island basalts (OIB). The values in excess of this range are generally attributed either to the presence of a recycled component in the Earth's mantle or to shallow level contamination processes. A viable way forward to trace source heterogeneity is to find a link between chemical (elemental and isotopic) composition of the earlier crystallized mineral phases (olivine) and the composition of their parental magmas, then using them to reconstruct the composition of source region. The Canary hotspot is one of a few that contains ~1-2 Ga old recycled ocean crust that can be traced to the core-mantle boundary using seismic tomography and whose origin is attributed to the mixing of at least three main isotopically distinct mantle components i.e., HIMU, DMM and EM. This work reports ion microprobe and single crystal laser fluorination oxygen isotope data of 148 olivine grains also analyzed for major and minor elements in the same spot. The olivines are from 20 samples resembling the most primitive shield stage picrite through alkali basalt to basanite series erupted on Gran Canaria, Tenerife, La Gomera, La Palma and El Hierro, Canary Islands, for which shallow level contamination processes were not recognized. A broad range of $\delta^{18}O_{olivine}$ values from 4.6 to 6.1‰ was obtained and explained by stable, long-term oxygen isotope heterogeneity of crystal cumulates present under different volcanoes. These cumulates are thought to have crystallized from mantle derived magmas uncontaminated at crustal depth, representing oxygen isotope heterogeneity of source region. A relationship between Ni×FeO/MgO and $\delta^{18}O_{olivine}$ values found in one basanitic lava erupted on El Hierro, the westernmost island of the Canary Archipelago, was used to estimate oxygen isotope compositions of partial melts presumably originated from peridotite (HIMU-type component inherited its radiogenic isotope composition from ancient, ~1–2 Ga, recycled ocean crust) and pyroxenite (young, <1 Ga, recycled oceanic crust preserved as eclogite with depleted MORB-type isotopic signature) components of the Canary plume. The model calculations yield 5.2 and 5.9±0.3‰ for peridotite and pyroxenite derived melts, respectively, which appeared to correspond closely to the worldwide HIMU-type OIB and

upper limit N-MORB δ^{18}O values. This difference together with the broad range of δ^{18}O variations found in the Canarian olivines cannot be explained by thermodynamic effects of oxygen isotopic fractionation and are believed to represent true variations in the mantle, due to oceanic crust and continental lithosphere recycling.

Keywords Canary Islands, oxygen isotopes, olivine, ion microprobe, SIMS, Laser fluorination

Introduction

Chemical and isotopic heterogeneity of the Earth's mantle is widely attributed to the temporal and spatial coexistence of isotopically enriched and depleted mantle domains (e.g. EM1, EM2, HIMU and DMM; Zindler and Hart 1986). This heterogeneity is thought to reflect time-integrated effects of depletion and enrichment caused by mantle partial melting and crust extraction and by subduction, and recycling of the oceanic lithosphere back into the convecting mantle (e.g. Hofmann and White 1982). The geochemistry of trace elements and radiogenic isotope data on ocean island basalts (OIB) provide powerful evidence that the convecting mantle is physically and chemically heterogeneous at very different scales. This also was demonstrated by recent seismic tomography data, where recycling of oceanic crust into the deep mantle due to subduction is a governing process for creating compositional heterogeneity, explaining the distinct geochemistry of mantle plumes (e.g. van der Hilst et al. 1991, 1997; Hofmann 1997).

Oxygen isotopes could be effectively used to trace crustal components in the source of basaltic magmas (e.g. Eiler et al. 1997a; Eiler 2001; Widom and Farquhar 2003; Bindeman et al. 2005; Bindeman 2008) because they vary strongly in the ocean crust, being later recycled back into the Earth's mantle. The oxygen isotope heterogeneity of the recycled ocean crust is generally caused by seawater and fluid alteration at high and low-temperatures (e.g. Alt et al. 1986; Muehlenbachs 1986; Taylor and Sheppard 1986). Being affected by low- and high-temperature fluid-rock interaction and due to cross-over of oxygen isotopic fractionation factors between minerals and water and their magnitude at around 300°C, the oceanic crust may vary significantly in oxygen isotope composition. During subsequent subduction and recycling, the relative proportions of ^{18}O-enriched and ^{18}O-depleted material has been shown to remain broadly similar to those in the ocean crust prior to subduction, leading to δ^{18}O values in the later erupted volcanic products to be distinct from that of pristine mantle (e.g. Bebout and Barton 1989; Putlitz et al. 2000).

The Canary hotspot can be traced to the core-mantle boundary using seismic tomography (Montelli et al. 2004) and whose origin is attributed to the mixing of relatively

old (1–2 Ga), HIMU-type upwelling hotspot mantle with the components of younger (<1 Ga), isotopically depleted (MORB)-type recycled ocean crust and isotopically enriched (EM)-type lithosphere (e.g. Hoernle and Tilton 1991; Hoernle et al. 1991, 1995; Marcantonio et al. 1995; Widom et al. 1999; Simonsen et al. 2000; Lundstrom et al. 2003; Gurenko et al. 2006 among others). The recycled component was shown to differ substantially in chemical and isotopic composition, being represented by relatively young, isotopically depleted, MORB-type ocean crust of the western Canary Islands (the islands of El Hierro, La Palma, La Gomera and Teno and Roque del Conde Massifs on Tenerife) versus the enriched, HIMU-type component mixed with EM-type asthenosphere or delaminated African subcontinental lithosphere of the eastern Canaries (Anaga Massif on Tenerife, Gran Canaria, Fuerteventura and Lanzarote; Gurenko et al. 2009, 2010). Because identification of source components is one of the major geochemical challenges of igneous petrology and as the HIMU- and EM2-type ocean island basalts (OIB) worldwide display the widest (1.4‰ i.e., from 4.7 to 6.1‰) range of bulk olivine oxygen isotopic composition (Eiler 2001), the composition of high-Mg olivines representing the first liquidus phases of primitive magmas erupted during the shield building stages of the Canary Islands can be used to investigate the scale of oxygen isotope heterogeneity in the Earth's mantle presumably caused different geochemical types of the recycled crust.

With the appearance of large radius, high transmission and high mass resolution instruments such as CAMECA IMS 1270-1280, substantial improvements of secondary ion mass spectrometry (SIMS) technique has been made during the last decade (e.g. Mojzsis et al 2001; Gurenko et al. 2001; Zeb Page et al. 2007; Chaussidon et al. 2008; Bindeman et al. 2008; Kita et al. 2009). The investigations of crystal domains of 10-30 μm size with precision of 0.3–0.5‰ (2σ SE, 2-sigma standard error) in a single spot analysis became feasible. A combination of *in-situ* SIMS technique with single grain laser fluorination (LF) analysis (giving 2σ analytical uncertainty of better than ±0.1–0.2‰) allowed precise detection of the contrasting in δ^{18}O source components for several Icelandic large volume Holocene basaltic eruptions (Bindeman et al. 2008) and, thus, it can be applied for discrimination between mantle and crustal processes.

This work reports the results of oxygen isotope study of 148 individual olivine phenocrysts from a suite of the most primitive picritic to basaltic and basanitic shield stage lavas from five of the seven Canary Islands (Gran Canaria, Tenerife, La Gomera, La Palma and El Hierro), as well as from submarine basaltic hyaloclastites of Site 953 drilled during the ODP Leg 157 to the NE of Gran Canaria (Gurenko et al. 1998, 2006). Unlike previous oxygen isotope studies of multiple grain olivine separates (e.g. Mattey et al. 1994; Eiler et al. 1997a; Turner et al. 2007 among others), in the present work we characterize a suite of large and Mg-rich olivine phenocrysts using single crystal laser fluorination and *in situ* ion microprobe oxygen isotope methods. Because oxygen diffision in olivines is relatively slow even at magmatic temperatures (e.g. Muehlenbachs and Kushiro 1974), we assume that each olivine core records δ^{18}O value of the incremental parental melt, from which it has crystallized. As shown by Bindeman (2008) and Auer et al. (2009), olivines having different chemical and O isotope composition and representing mantle domains, from each the parental basalting magma was extracted, can be found in the same lavas, brought together by rapid mixing processes in magma plumbing systems.

Several recent studies (Sobolev et al. 2008; Gurenko et al. 2009, 2010) have demonstrated distinct relationships between estimated peridotite-to-pyroxenite proportions in the source regions and the Sr, Nd, Pb and Os radiogenic isotope compositions of the lavas. In the present work, we use the model suggested by Sobolev et al. (2007) that allows to assign each individual olivine crystal or even its growth zone to the composition of parental melt, for which the peridotite/pyroxenite ratio can be calculated. The aim of the study is to constrain oxygen isotope composition of the peridotite and pyroxenite components in the mantle beneath the Canary Islands, by defining the relationships between Ni and Mn concentrations in *individual* olivine grains and their oxygen isotope ratios, as has previously been shown for radiogenic isotopes (Gurenko et al. 2009, 2010).

Geological setting and samples studied

The Canary Archipelago (**Fig. 1**) has a long magmatic history ranging from at least 20 Ma

in the easternmost Canary Islands through 12–16 Ma in the central part of the archipelago to less than 1 Ma on the westernmost islands, representing an age-progressive, ~500 km long island chain. Volcanic rocks from the Canary Islands are characterized by a large compositional range from moderately alkaline basalts and picrites, which are dominant in the shield-building stage to olivine nephelinites and basanites of the later (post-erosional or rejuvenated) stage of volcanism. Although shallow depth magma contamination is a common process for the Canary Island volcanoes (e.g. Thirlwall et al. 1997; Gurenko et al. 2001; Hansteen and Troll 2003; Longpré et al. 2008 and references therein), the samples selected for the present study show no evidence for extensive crustal contamination based on our previous studies of major and trace elements, stable and radiogenic isotopes (Gurenko et al. 2006, 2009, 2010).

We selected Mg-rich olivine phenocrysts of $Fo_{80.3\text{-}89.8}$ covering almost the entire range of Ni (0.169–0.480 wt.% NiO) and Mn (0.145–0.274 wt.% MnO) concentrations (**Fig. 2a, b**) known for Canary Island lavas. Our selection is based on nearly 1450 previously analyzed individual olivine grains from 17 subaerially erupted transitional basalts and picrites and three olivine-phyric basanites representing volcanic shields on Gran Canaria, Tenerife, La Gomera, La Palma and El Hierro (geographic coordinates, petrographic description, chemical and isotopic compositions of the rock samples are given in Gurenko et al. 2006), as well as from three samples representing the Gran Canaria volcaniclastic apron drilled during the ODP Leg 157 (Gurenko et al. 1998, 2009, 2010).

Analytical technique

The *in-situ* $^{18}O/^{16}O$ ratios in olivine crystals were analyzed with the CAMECA IMS 1270 ion microprobe in the *Centre de Recherches Pétrographiques et Géochimiques* (CRPG, Nancy, France). The laser fluorination data were acquired in the Stable Isotope Laboratory of the University of Oregon (Eugene, USA; Bindeman 2008; Bindeman et al. 2008).

Sample preparation

Olivine samples analyzed with SIMS were mounted together with reference San Carlos and CI114 olivines in the central part (½ inch in diameter) of 1-inch epoxy resin mounts. The mounts were then ground and finally polished using the 6, 3, 1 μm grain size Diamond Films and Glass Support Plates of the ALLIED High Tech Products company. As shown by Kita et al. (2009), such sample preparation technique allows minimizing effectively the relief difference between the embedded olivine grains and enclosing epoxy resin.

The lavas studied here contain abundant and large (up to 5–10 mm) olivine phenocrysts, which may be partly altered outside and along their fractures filled by light green to colorless clay minerals and serpentine or by iddingsite (mixture of clay minerals with iron oxides and ferrihydrites). All olivines were thus carefully investigated under transmitted and reflected light using petrographic (thin sections) and binocular (monomineral fractions) microscopes and only visually fresh crystals were selected for the study. The largest crystals to be analyzed with both SIMS and LF methods were split and one of two parts was analyzed by laser fluorination. The grains selected for SIMS were imaged in secondary (SE) and back-scattered electrons (BSE) to ensure that the surfaces are free of secondary alteration products. The olivine parts to be analyzed by LF were crushed and cleaned in 30% HF or in HFB_4 solutions for variable amounts of time. Some visually fresh olivines sent for LF analyses appeared dull during more careful investigations under the binocular microscope. Given that this may be a sign of internal serpentinization, these grains were additionally subjected to element mapping under the electron microprobe in order to target the freshest crystal domains suitable for analyses by SIMS (SE images and Mg, Si and Ni X-ray maps of the selected representative olivine grains are given in the *On-line Supplementary Information;* **Fig. S1**). Because of such olivine alteration, the SIMS technique, which gives better spatial resolution compared to laser fluorination, was chosen as a preferred method of oxygen isotope analysis. The LF method, although being analytically more precise, was used to demonstrate that both SIMS and LF methods are in good agreement with each other. Finally, the spots analyzed by SIMS were then re-analyzed by electron microprobe using a high precision technique described by Sobolev et al. (2007). All these replicate analyses showed stoichiometric

olivine compositions, also suggesting that our SIMS oxygen isotope dataset does not contain analyses of altered olivines.

IMS 1270 setting

Olivines were sputtered with a 10 kV Cs^+ primary beam of ca. 10 nA current focused to 10–20 μm spots after pre-sputtering time of 120 s. The normal-incidence electron flood gun was used to compensate for sample charge. Secondary $^{16}O^-$ and $^{18}O^-$ ions were accelerated at 10 kV and analyzed at a mass resolution of 2,500 using a circular focusing mode and a transfer optic of about 150 μm. The energy slit was centered and opened to 50 V. The automatic routine of centering secondary beam in the field aperture was used at the beginning of each isotopic measurement. The $^{18}O/^{16}O$ isotopic ratios were analyzed in multi-collection mode using two off-axis L'2 and H1 Faraday Cup (FC) detectors for counting the ^{16}O and ^{18}O ion intensities simultaneously. The gain of the Faraday cups was calibrated daily at the beginning of each analytical session using the CAMECA built-in amplifier calibration software, and the signal was then corrected for the FC backgrounds. Typical ion intensities of ca. $2–5\times10^9$ and $4–9\times10^6$ counts per second (cps) obtained on the ^{16}O and ^{18}O peaks, respectively, yield an internal 1σ uncertainty of better than ±0.1‰ which was reached after ~100 s of counting (50 cycles of 2 sec of analysis time each).

Instrumental mass fractionation

Instrumental mass fractionation (IMF) is usually defined as the ratio between measured and true values:

$$\alpha_{IMF} = R_{measured} / R_{true}, \quad (1)$$

or can be reported in permil units calculated using the relationship:

$$IMF = [(R_{measured} - R_{true}) / R_{true}] \times 1000‰, \quad (2)$$

where R stands for $^{18}O/^{16}O$ ratios in this study. Previous work has shown that there is a clear relationship between IMF of O isotopes and chemical composition of the analyzed material, especially while using the small-radius CAMECA IMS 4f–6f instruments (e.g. Valley and Graham 1991; Eiler et al. 1997b). The large radius multicollector CAMECA IMS 1270–1280 instruments, in contrast, ensure a smaller and better predictable IMF (Mojzsis et al 2001; Gurenko et al. 2001; Zeb Page et al. 2007; Chaussidon et al. 2008; Bindeman et al. 2008; Kita et al. 2009).

Because our unknown olivines range in forsterite content from ~Fo_{80} to Fo_{90}, we used two reference olivines with strongly contrasting Fo contents. The first is San Carlos olivine (*SCO*; we used the same aliquot of material that was analyzed by concurrent laser fluorination) with $\delta^{18}O$ value of 5.35‰ determined previously by laser fluorination in Caltech (Eiler 2001; Bindeman et al. 2006) that was mounted separately and together with the samples of interest. No grain to grain variability in O isotope ratios was found within a common analytical precision of ±0.2–0.4‰ (2σ SE) obtained for CAMECA IMS 1270 analysis during this study (see below). The second reference olivine (*CI114*) is from a piece of olivine-anorthite cumulate nodule from Zheltovsky volcano, Kamchatka. It reveals insignificant grain-to-grain compositional variability ranging in forsterite content from $Fo_{74.1}$ to $Fo_{74.4}$. The $\delta^{18}O$ value of the CI114 olivine (5.2 ± 0.2‰, 2σ SE) has also been previously determined by the laser fluorination technique (Bindeman et al. 2008).

Similarly as shown by Bindeman et al. (2008), we do not observe a systematic difference in IMF value obtained on SCO with $Fo_{90.7}$ and CI114 with $Fo_{74.2}$ ($\Delta IMF_{sco-ci114}$) as a function of Fo content obtained during three analytical sessions in May-2006, June-2007 and July-2007, ranging from –0.31 to +0.57‰ at average $\Delta IMF_{sco-ci114}$ = 0.07 ± 0.58‰, 2σ SD. Note that the relatively high standard deviation of 0.58‰ represents, in fact, a propagation of the uncertainties obtained on SCO and CI114 reference olivines. These values are very close to those obtained by Bindeman et al. (2008; $\Delta IMF_{sco-ci114}$ = 0.12 ± 0.70‰) (**Fig. 3a**). Because the absolute value of $\Delta IMF_{sco-ci114}$ is small, we did not introduce the IMF correction as a function of Fo content and used the average of IMF

values obtained on both reference olivines, correcting our raw data for instrumental drift where present.

Precision and accuracy

Secondary ion mass spectrometry

Three to 5 individual $\delta^{18}O$ measurements were run on each of the two olivine standards at the beginning and at the end of each block of data acquisition, including three to five unknown samples (total 15 to 20 spots) employing so-called "contiguous bracketing". To correct raw data for IMF, we used an average value of IMF derived from the measurements at the beginning and the end of a given data block, where no instrumental drift was observed. If a systematic shift of IMF values during one or several data blocks was observed (usually it is 0.05 to 0.1‰ per hour), the unknown data were corrected for IMF calculated as a function of time within these data blocks. The uncertainties on SCO and CI114 were nearly identical i.e., ±0.23‰ on SCO vs. ±0.22‰, 2σ SD on CI114, when run together in the same data blocks and obtained on multiple grains mounted together with unknown olivines. This observed similarity suggests that both standards are equally homogeneous and instrument stability was maintained.

The error of a single measurement of an unknown sample was defined from two sources of independent random errors. One source is an internal precision of the instrument (±0.08–0.20‰, 2σ SE). Another source is represented by external reproducibility of the measurements of reference olivines and characterizes the accuracy of IMF determinations (0.10–0.46‰, 2σ SD). The accounted average cumulative analytical error (precision + accuracy) of a single O isotope measurement with the CRPG-Nancy CAMECA IMS 1270 instrument is thus ±0.35‰ (ranging from 0.22 to 0.52‰ for the total 373 measurements). Replicate measurements of the San Carlos olivine standard treated as an unknown sample have demonstrated the same reproducibility (5.30±0.34‰, 2σ SD, N = 12). We emphasize however that because each $\delta^{18}O$ analysis results from N = 2–5 replicate measurements, the analytical uncertainty of $\delta^{18}O$ of an individual olivine grain is $1/\sqrt{N}$ times better than the

297 uncertainty of a single measurement (i.e. 0.14–0.4‰, average ±0.24‰; **Table S1,** *On-line*
298 *Supplementary Information*).
299
300 *Laser fluorination*
301 Based on the concurrent multiple runs of the Gore Mountain Garnet (UWG-2, $\delta^{18}O$ =
302 5.8‰; Valley et al. 1995) primary and San Carlos olivine (SCO-2, $\delta^{18}O$ = 5.35‰; Eiler
303 2001; Bindeman et al. 2006) secondary reference materials, the precision of the single
304 crystal LF technique was always better than ±0.18‰ (2σ SD).
305
306 SIMS vs. LF
307 Twenty large individual olivine grains (up to 10 mm) were split and then analyzed by both
308 SIMS and LF methods. Our initial LF analysis of uncrushed and minimally HF-treated
309 bulk olivines (large grains and mixtures of grains) returned $\delta^{18}O$ values ranging from 3.8 to
310 4.9‰. The values appeared to be systematically lower than those of the SCO olivine
311 standard analyzed concurrently (5.28 ± 0.18‰ 2σ SD, N=15) or *in situ* analyses of the
312 freshest spots in the same olivines by SIMS (**Table S1;** *On-line Supplementary*
313 *Information*).
314 Given that olivine phenocrysts may contain single to several tens of small (5-50
315 μm) chromite crystals and chromite may hypothetically decrease the resulting $\delta^{18}O$ values,
316 as suggested in several stable isotope laboratories, we investigated this possibility. We
317 extracted pure chromite from multiple olivine phenocrysts of sample LP1 and analyzed it
318 by LF. While $\delta^{18}O$ value of this chromite was found to be 3.43‰ and the purest chromite-
319 free olivine has $\delta^{18}O$ = 4.89‰, the measured $\delta^{18}O$ value of the mechanical mixture
320 composed in weight proportion of 0.13 chromite and 0.87 chromite-free olivine was
321 4.51‰ (at predicted $\delta^{18}O$ of 4.69‰). Because (1) the chromite inclusions and host olivine
322 appear to be in isotopic equilibrium and (2) 13 wt% of inclusions to be trapped by olivine
323 is unrealistically high amount, as compared to what we observe in reality, the effect of

occasionally trapped chromite inclusions on the oxygen isotopic composition of the studied Canary olivines was found to be negligible.

Thus, we think that the systematically lower $\delta^{18}O$ values obtained with LF method were caused more probably by crack/cleavage serpentinization (observed in some grains under high power magnification) and we attempted to remove this by crushing each olivine grain to 100-150 um fraction and subjecting it to 24 hour treatment in HBF_4. Indeed, the $\delta^{18}O$ values obtained for nine HBF_4 treated olivine grains during subsequent LF analytical session in October 2006, where the material was crushed to a smaller size and subjected to substantially longer time of leaching in HBF_4 (about 24 hours), have demonstrated better correlation with SIMS data (**Table S1;** *On-line Supplementary Information*). Furthermore, the additional LF oxygen isotope compositions of 25 arbitrary selected, freshest olivine crystals were obtained in January 2010. Although these olivines were not subsequently analyzed by SIMS (but they were analyzed for major and minor elements by electron microprobe), all they are within the previously obtained ranges of oxygen isotope composition (**Table S1;** *On-line Supplementary Information*).

Finally, these nine Canarian olivines analyzed by both LF and SIMS methods were combined with seven olivine grains from the basaltic lava flow of the 1783–1784 AD fissure eruption of Laki (Iceland) also analysed by LF and SIMS (Bindeman et al. 2008) and plot together in **Fig. 3b**, demonstrating very good correspondence of both methods on the SMOW scale. Due to high spatial resolution, we therefore think that SIMS analysis of multiple freshest 10-20 um spots in individual olivines cores represents true analytical dataset for the Canary olivines (**Table S1;** *On-line Supplementary Information*).

Oxygen isotope composition of the Canarian olivines

The $\delta^{18}O$ values of a total of 148 olivine phenocrysts are listed in **Table S1 (***On-line Supplementary Information*). As no systematic difference observed for the $\delta^{18}O_{olivine}$ sets obtained by SIMS and LF methods, we choose to discuss them as a single dataset. The broad $\delta^{18}O_{olivine}$ range obtained by both LF and SIMS methods is between 4.6 and 6.1‰. In

several lava samples, the variations of $\delta^{18}O_{olivine}$ span almost the entire oxygen isotope range reported previously for the Canarian olivines in general (from 4.3 to 5.8‰ by Thirlwall et al. 1997; Gurenko et al. 2006; Day et al. 2009, 2010; **Fig. 4**), while the highest value in the range that we obtain here correspond nearly exactly to the highest $\delta^{18}O$ measured in clinopyroxene from Gran Canaria by Thirlwall et al. (1997). No significant intra-crystal $\delta^{18}O_{olivine}$ or Fe-Mg variations in the cores of individual olivines are observed, except for four olivine grains exhibiting variations of 0.1–0.7 mole % Fo and 0.6–0.9‰ $\delta^{18}O_{olivine}$ (**Table S1,** *On-line Supplementary Information*). Because of the large broad $\delta^{18}O_{olivine}$ range (i.e. 1.5‰), especially that observed for the Tenerife, La Gomera and La Palma series (it is about six times larger than the 2σ analytical uncertainty of SIMS), we interpret it as representing true oxygen isotope heterogeneity of parental magmas.

The $\delta^{18}O_{olivine}$ values, either those obtained by SIMS or LF, are scattered (**Fig. 5**). The intervals obtained for the El Hierro (5.21 ± 0.40%, 2σ SD) and La Palma (5.48 ± 0.71‰, 2σ SD) samples are wider, as well as the average $\delta^{18}O_{olivine}$ value for La Palma is higher, than those reported by Day et al. (2009, 2010) (5.17 ± 0.16‰ El Hierro and 4.87 ± 0.36‰ La Palma, 2σ SD). Given that our earlier obtained LF data for the set of La Palma olivines (where HF leaching appeared to be too short for complete removal of the alteration products) tends to the systematically lower $\delta^{18}O_{olivine}$ values than those we finely report as true, we think that the remaining alteration of olivine may be also a possible reason for the lower La Palma $\delta^{18}O_{olivine}$ reported by Day et al. (2009, 2010).

The $\delta^{18}O_{olivine}$ range obtained during this work is much wider than that of typical MORB, OIB, oceanic and continental peridotites (5.0–5.4‰) based on multiple grain olivine separates by Mattey et al. (1994), Eiler et al. (1997a); and Turner et al. (2007) but is still bracketed by the intervals defined for olivine phenocrysts from the HIMU- and EM2-type lavas ($\delta^{18}O_{olivine}$ = 4.6–5.1‰ and 5.4–6.1‰, respectively; Eiler et al. 1997a; Widom and Farquhar 2003) and is much narrower than the global $\delta^{18}O_{olivine}$ range (2.2 to 7.6‰) based on the single grain olivine analysis by laser fluorination (Bindeman 2008).

There are no clear relationships between O isotopic compositions and Fo contents for olivines from the lavas erupted on the western Canaries, except for one El Hierro

olivine series showing decrease of $\delta^{18}O_{olivine}$ values with increasing Fo (R^2 = 0.36; **Fig. 5a**). This olivine series shows also a subtle correlation (R^2 = 0.29) between $\delta^{18}O_{olivine}$ and Ni×FeO/MgO ratios but with the opposite slope (**Fig. 5d**). No correlation of $\delta^{18}O_{olivine}$ with Mn/FeO ratios was found for any of the studied olivine series.

Do oxygen isotope variations in olivines represent mantle or crustal signature?

Two concurrent processes, i.e. magma contamination due to interaction with upper crustal rocks and/or partial melting of a mantle source with variable oxygen isotope signatures, could potentially account for the observed range of oxygen isotope ratios.

Large variations of $\delta^{18}O_{cpx}$ (cpx = clinopyroxene) values (5.2 to 6.8‰) obtained for a narrow range of $^{87}Sr/^{86}Sr$ isotope ratios (0.7032 to 0.7039) in the Gran Canaria shield basalts were reported by Thirlwall et al. (1997) who suggested up to 8% assimilation of the NW African passive margin sediments by these magmas. Gurenko et al. (2001), using the relationships of $\delta^{34}S$ vs. $\delta^{18}O$ recorded in clinopyroxene-hosted glass inclusions from the Miocene basaltic hyaloclastites drilled at Site 956 during the ODP Leg 157 southwest of Gran Canaria, have proposed assimilation of anhydrite-bearing, hydrothermally altered basaltic crust and oceanic sediments by ascending primary magmas. Thus, magma contamination by lower crustal rocks and/or marine sediments is probable during the shield building stage of the Canary Islands, especially for the case of Gran Canaria. On the other hand, Gurenko et al. (2006) have demonstrated that many primitive picritic to alkali basaltic shield stage lavas form Gran Canaria, Tenerife, La Gomera and La Palma (including all samples studied here) lack crustal contamination based on Sr-Nd-Pb and bulk olivine $\delta^{18}O$ vs. Sr isotope relationships, consistent with our present data (**Fig. 6)**. The only exception could be sample G1265 (Hoernle et al. 1991; Gurenko et al. 2006) representing the Gran Canaria shield stage, for which only a small (less that 2%) contamination by marine sediments might be invoked.

Recent studies of the low-$\delta^{18}O$ basaltic magmas in Iceland (Bindeman et al. 2008) and Hawaii (Wang and Eiler 2008) have demonstrated that the decrease of O isotope ratios

409 with decreasing Fo content of individual olivine grains may be caused by assimilation of
410 low-δ^{18}O lithospheric rocks by ascending magmas (*Contamination* trend shown in **Fig. 5a-**
411 **c**). We can only vaguely recognize such trend in subaerial lavas from Gran Canaria (**Fig.**
412 **5b**), which may suggest that δ^{18}O-depleted crustal rocks might have been assimilated by
413 the magmas with originally "normal mantle" δ^{18}O values. Indeed, lower crustal gabbroic
414 xenoliths with normal to moderately low δ^{18}O values (3.3–5.1‰) are known on Gran
415 Canaria (Hansteen and Troll 2003). These xenoliths are characterized, however, by varying
416 to somewhat elevated $^{87}Sr/^{86}Sr$ ratios (0.7029–0.7047; Hoernle 1998). Assimilation of such
417 crustal material will drive the composition of the hybrid magmas towards lower δ^{18}O and
418 higher $^{87}Sr/^{86}Sr$ values, the tendency which is opposite to the common trend of δ^{18}O
419 increase with increasing $^{87}Sr/^{86}Sr$ (e.g. Thirlwall et al. 1997). However as shown by
420 Gurenko et al. (2006), assimilation of prohibitively large amounts of such lower crustal
421 material (up to 70%) is required and this is not supported by Pb isotope data. We therefore
422 do not consider crustal assimilation as a likely explanation for the observed large range of
423 $\delta^{18}O_{olivine}$ values from 4.6 to 6.1‰.

424 The better explanation of diverse δ^{18}O in the Canarian olivines is provided by a
425 model in which different lavas are formed by variable degree decompression melting of a
426 HIMU-type mantle (e.g. Hoernle and Tilton 1991; Hoernle et al. 1991, 1995; Marcantonio
427 et al. 1995; Widom et al. 1999; Simonsen et al. 2000; Lundstrom et al. 2003 among others)
428 that may contain a depleted MORB-type component of recycled oceanic crust in the form
429 of reaction pyroxenite mixed with EM-type peridotitic component from the asthenosphere
430 or lithosphere above the plume center (Gurenko et al. 2009, 2010). In particular, the
431 Ni×FeO/MgO, Mn/FeO ratios and Ca concentrations of olivine phenocrysts correlate well
432 with bulk-rock Sr, Nd and Pb isotopic compositions of their host lavas (Gurenko et al.
433 2009, 2010). As shown by Gurenko et al. (2009), the radiogenic Sr, Nd and Pb isotope
434 ratios of mafic, relatively low-silica (SiO_2 <46) alkali basaltic to basanitic lavas from the
435 western Canary Islands form arrays between the HIMU-like and mid-ocean-ridge basalt
436 (MORB) or DMM (Zindler and Hart 1986) end-members, interpreted to reflect (i)
437 interaction of plume-derived melts with depleted upper mantle (Hoernle et al. 1991, 1995),

or (ii) mixing between older (HIMU-like) and younger (MORB-like) recycled oceanic crustal components to be present either within a single plume (Widom et al. 1999; Gurenko et al. 2009) or in an upwelling asthenosphere (Geldmacher et al. 2005). In addition, more Si-rich (SiO_2 >46) transitional basaltic and evolved magmas erupted on the eastern Canary Islands (i.e., Lanzarote, Fuerteventura, Gran Canaria and Anaga Massif on Tenerife) show evidence for the presence of a third, enriched-mantle (EM)-type component that can be located in the shallow asthenosphere or lithosphere, having been entrained by the ascending mantle plume (Hoernle and Tilton 1991; Hoernle et al. 1991, 1995; Widom et al. 1999; Simonsen et al. 2000; Lundstrom et al. 2003; Gurenko et al. 2006, 2009, 2010). Alternatively, melting of peridotitic mantle metasomatised by <10% pyroxenite/eclogite made from variable portions of similar aged recycled oceanic crust and lithosphere with HIMU affinities have been recently proposed by Day et al. (2009, 2010). The obtained large range of $\delta^{18}O_{olivine}$ values from 4.6 to 6.1‰ can thus be interpreted as reflecting mantle source signature and not being produced by shallow depth contamination by crustal rocks. We next focus on identifying the ^{18}O-enriched and ^{18}O-depleted sources that contributed to the observed $\delta^{18}O_{olivine}$ heterogeneity in the Canarian plume.

Oxygen isotope composition of the peridotite and pyroxenite derived melts in the source of El Hierro magmas

Olivine from mantle xenoliths, mid-ocean ridge and most ocean island basalts generally show a relatively narrow range of oxygen isotopic ratios ($\delta^{18}O_{olivine}$ = 5.0–5.4‰; Mattey et al., 1994). The values in excess of this range, as those from the lavas exhibiting EM2 ($\delta^{18}O_{olivine}$ = 5.4–6.1‰) and HIMU ($\delta^{18}O_{olivine}$ = 4.7–5.1‰) reservoirs (Eiler et al. 1997a; Eiler 2001), or that of island arc magmas, are commonly attributed to the presence of recycled crust in the source of magmas, which may possess both high-δ^{18}O and low-δ^{18}O signatures due to suspected low- and high-temperature surface processes or interacting with seawater (e.g. Alt et al. 1986; Muehlenbachs 1986; Taylor and Sheppard 1986). Recent studies also have suggested that high- and low-δ^{18}O values of mantle olivines may

466 be related to either direct recycling of sediments and the upper portions of the slabs (high
467 δ^{18}O) or their interior portions (low-δ^{18}O) (e.g. Turner et al. 2007; Day et al. 2009, 2010).
468 Slab partial melts or slab-derived metasomatic agents, both being siliceous, would react
469 with peridotite forming variable in δ^{18}O pyroxenitic veins. It is also possible that high and
470 low δ^{18}O signatures counterbalance each other and lead to the "normal mantle" δ^{18}O
471 average, as observed in adakites by Bindeman et al (2005). Because oxygen is a major
472 element with approximately the same concentration in most known terrestrial silicate
473 reservoirs, and deeply subducted oceanic crust appears to retain both 18O-enriched and
474 18O-depleted components, each in relative proportions and with δ^{18}O values broadly
475 similar to those in the crust prior to subduction (e.g. Bebout and Barton 1989; Putlitz et al.
476 2000), isotopic variations in the rocks can be interpreted as reflecting mass proportions of
477 the contributing source components. However, these high and low δ^{18}O portions can be
478 mechanically or convectively separated in the mantle yielding diverse in δ^{18}O partial melts.
479 In the approach discussed below, we consider each individual olivine crystal (or
480 even a smaller domain analyzed by SIMS) with known δ^{18}O as having crystallized from a
481 given portion of a hybrid magma, originated from mixing of peridotite and pyroxenite
482 derived partial melt fractions having different Sr-Nd-Pb isotopic composition, and their
483 relative proportions can be inferred from Ni (and Mn) concentrations of this olivine
484 (Gurenko et al. 2009, 2010). Such approach is particularly warranted because the observed
485 Fo, Ni, Mn and Ca heterogeneity of olivines from each individual rock sample suggest that
486 these olivines may represent entrained cumulates crystallized from diverse basaltic
487 magmas (Gurenko et al. 2006). In this context, each olivine crystal is treated as a
488 messenger of chemical and isotopic variations of parental magmas and consequently their
489 source regions. Furthermore, chemical composition of olivine (expressed in terms of Ni
490 and Mn concentrations and their ratios) and oxygen isotope ratio analyzed in the same spot
491 can be directly assigned to the proportions and isotopic values of the peridotitic and
492 pyroxenitic components in the magma source.
493 We observe that for the entire Canary Island hot spot track, there is no simple,
494 Canary-wide relationship between $\delta^{18}O_{olivine}$ values and inferred fraction of the pyroxenite

endmember, as compared to such correlations observed for Sr-Nd-Pb radiogenic isotopes of the eastern and western Canary Islands (Gurenko et al. 2009, 2010), most consistent with a conclusion that both peridotite and pyroxenite components might vary in oxygen isotope composition. Only the olivine phenocrysts from one lava (EH4 basanite from El Hierro) show subtle linear correlations between $\delta^{18}O_{olivine}$ and Fo contents (R^2 = 0.36, opposite to the *Contamination* trend taken from Wang and Eiler 2008) and Ni×FeO/MgO ratios (R^2 = 0.29), both being however significant at 95% confidence level (**Fig. 5a, d**). In overall, we suggest that the dataset can be explained by mixing of (i) peridotite with "normal mantle" or slightly lower $\delta^{18}O$ values, (ii) high-$\delta^{18}O$ pyroxenite likely derived from the top of the recycled ocean crust and (iii) low-$\delta^{18}O$ component also having crustal (the interior portion of the slab) or lithospheric origin, in accordance with models proposed by Day et al. (2009, 2010) and Gurenko et al. (2009, 2010). In this context, the El Hierro basanite, whose Sr-Nb-Pb radiogenic isotope composition reflects a mixture of only two, the most extremely enriched (HIMU)-type peridotite and depleted (MORB)-type pyroxenite components (Gurenko et al. 2009), represents an exceptional case to assess directly the scale of oxygen isotope heterogeneity of the distinct mantle domains.

To calculate relative contribution of the peridotite and pyroxenite components to primary magma origin during partial melting, we used the equation taken from Gurenko et al. (2009):

$$X_{px} = 1.341E{-}03 \times [Ni{\times}FeO/MgO] - 0.437$$

where X_{px} = weight fraction of pyroxenite derived melt (given in **Table S1,** *On-line Supplementary Information*). The regression relating $\delta^{18}O_{olivine}$ and calculated X_{px} values was used to estimate oxygen isotope compositions in the postulated peridotite and pyroxenite derived end-members (**Fig. 6**). Then, if we consider the compositions of olivine as plotting along a single mixing line, extrapolating it to X_{px} = 0 and 1 in **Fig. 6**, we obtain that the enriched (HIMU)-type peridotitic and the depleted (MORB)-type pyroxenitic end-members are characterized by distinct $\delta^{18}O_{olivine}$ values of 4.8 and 5.5 ± 0.3‰,

524 respectively. The 0.3‰-uncertainty was calculated assuming two sources of independent
525 random errors (Taylor 1982): (1) the 2σ analytical errors of individual measurements
526 (given in **Table S1,** *On-line Supplementary Information*) and (2) the uncertainty caused by
527 deviations of the measured isotope ratios from the regression line, calculated as:
528
529 $$\sigma_y^2 = \frac{1}{N-2}\sum_{i=1}^{N}(y_i - Ax_i - B)^2 ,$$
530
531 where A and B are constants in linear regression ($y = A \times X_{px} + B$), N = number of points.
532 Finally, using the oxygen isotope equilibrium fractionation factor ($\Delta_{olivine–melt}$) of 0.4‰
533 (Eiler 2001) and converting the obtained $\delta^{18}O_{olivine}$ values into those of the corresponding
534 silicate liquid endmembers, we obtain $\delta^{18}O_{melt}$ of 5.2‰ for (HIMU)-type peridotite and
535 5.9‰ for (MORB)-type pyroxenite derived melts. Our present estimations broadly
536 correspond to the worldwide HIMU-type OIB and the upper limit N-MORB $\delta^{18}O$ values
537 (Eiler et al. 1997a; Eiler 2001). The $\delta^{18}O_{melt}$ of 5.9‰ obtained for the pyroxenitic
538 component, which is somewhat higher than that of typical N-MORB, may reflect possible
539 high-temperature metamorphic reactions occurring during subduction and recycling.
540
541 **Effects of O isotope fractionation during partial melting**
542 We next address the question of whether the ~0.7‰ $\delta^{18}O$ difference between peridotite and
543 pyroxenite melt endmembers regressed in **Fig. 6** is due to possible thermodynamic effects
544 of oxygen isotopic fractionation between partial silicate melt and residual mineral phases
545 in the source. We have calculated a range of $\delta^{18}O$ values of the modeled peridotite and
546 pyroxenite partial melts as a function of (i) source mineralogy, (ii) degree of partial
547 melting, and (iii) fractionation of oxygen isotopes between silicate minerals and melts. The
548 effects of two extreme mechanisms of partial melting i.e., modal batch and fractional
549 (Shaw 1970) were then compared (**Table 1**).
550 The $\delta^{18}O$ values of melts as a function of partial melting degree were calculated
551 assuming initial $\delta^{18}O_{init}$ = 4.8‰ for peridotite (i.e. “olivine equivalent” value obtained for

552 the peridotite endmember of El Hierro; **Fig. 6**) and varying $\delta^{18}O_{init}$ values for pyroxenite
553 (4.6‰ being equal to the minimum $\delta^{18}O_{olivine}$ value of the entire data set, 4.8‰, as that of
554 peridotite and 6.1‰, the highest $\delta^{18}O_{olivine}$ of the data set). Assuming oxygen isotope
555 equilibrium between mineral and melt phases during the entire partial melting event, we
556 treated oxygen isotope fractionation factors similarly as distribution coefficients of
557 incompatible elements, using a set of equilibrium fractionation factors of oxygen isotopes
558 between olivine, clinopyroxene, orthopyroxene, garnet and coesite and picrite melt
559 [$\alpha_{mineral-melt} = (^{18}O/^{16}O)_{mineral}/(^{18}O/^{16}O)_{melt}$] taken from Eiler (2001), arbitrary assigning
560 $\alpha_{quartz\text{-}melt}$ to coesite (**Table 1**). The proportions of mineral phases together with partial
561 melting degrees were taken directly from experiments of Walter (1998) for garnet
562 peridotite and Yaxley and Sobolev (2007) and Sobolev et al. (2007) for pyroxenite. These
563 experiments were performed at high magmatic temperatures and within their relatively
564 narrow interval (1400–1650°C; **Table 1**). The proportions of mineral phases did not
565 change significantly in this temperature interval. This justifies using the selected mineral-
566 melt fractionation factors as constant values.

567 The results of the modeling could be summarized as following. Within a wide
568 range of partial melting degrees (up to 42%), melting of peridotite and pyroxenite mantle
569 sources having the same oxygen isotope composition (i.e., $\delta^{18}O$ = 4.8‰) but differing
570 significantly in mineral compositions causes less than 0.2‰ difference in the resulting
571 partial melt $\delta^{18}O$ values (**Table 1, Fig. 7**). Larger degree of pyroxenite partial melting, as
572 compared to peridotite, which follows from systematically lower temperature of the
573 pyroxenite solidus (i.e., 25–45% of pyroxenite vs. 4–15% of peridotite; Sobolev et al.
574 2005), cannot account for the observed ~0.7‰ difference. This implies that the anticipated
575 peridotite and pyroxenite endmembers in the Canarian magma source possess a difference
576 of at least 0.5‰ for the case of the El Hierro magma source. Given the broad range of
577 $\delta^{18}O_{olivine}$ values found in the Canarian lavas, the oxygen isotopic difference between
578 distinct mantle domains of the Canary plume may be as large as 1.5‰.

579 In conclusion, we note that the results of the modeling are valid, if equilibrium
580 between coexisting mineral and liquid phases was reached during partial melting and melt

extraction. If separation of partial melts from a melting zone would have occurred more rapidly (for which we however don't have direct evidence), the resulting oxygen isotope disequilibria between the involved solid and liquid phases may affect the model outcome. Finally, we conclude that the observed oxygen isotope range is impossible to explain by varying oxygen isotope fractionation factors and conditions of partial melting and, as proposed above, two (as in the case of El Hierro), three or even more isotopically distinct peridotitic and pyroxenitic components are required.

Implications for magma underplating

Although the broad $\delta^{18}O_{olivine}$ range found in several individual picrite and basalt lavas from the Canary Islands (up to 1.2‰, **Fig. 4**) is not as large as measured in single eruptive units in Iceland or Kamchatka (ca 1-4‰, Bindeman et al. 2008; Auer et al. 2009), this may have an important implication for magma residence time, cumulate formation and storage in the magma plumbing system beneath the Canaries.

As we demonstrated above, the observed oxygen isotope heterogeneity of olivine crystals is ultimately attributed to the composition of their parental magmas, which in turn reflect the composition of their mantle sources. If so, these magmas remained unmixed in the magma plumbing system during the entire ascent from the deep source region (about 100 km depths; Gurenko et al. 1996) to the shallower depths (<15 km in accordance with fluid inclusion data; Gurenko et al. 1996, 1998). This conclusion is in agreement with a channeling melt percolation model proposed by McKenzie (1985), Williams and Gill (1989), Eggins (1992), being also independently supported by widely observed trace element heterogeneities preserved in mineral-hosted melt inclusions (e.g. Sobolev and Shimizu 1993, Gurenko and Chaussidon 1995; Sobolev et al. 2000). More recent detailed mineralogical studies (Longpré et al. 2008) also provide evidence for decompression-induced crystallization of the Canarian magmas upon rapid ascent.

Crystallization of such magmas generates crystal cumulates with variable $\delta^{18}O$ signature, which then are stored in the magma plumbing system. If subsequent magma

609 batches re-entrain such cumulates, transporting them to the surface, this may create isotope
610 diversity between individual crystals, as in the case of the studied Canary Island lavas.
611 Later partial isotopic and trace elemental re-equilibration of these olivines with the
612 transporting magmas due to intracrystalline solid diffusion (Costa and Chakraborthy 2004)
613 is unlikely because (a) these olivines exhibit wide ranges in Fo contents in the cores, (b)
614 concentrations of Ni, Mn and Ca in olivine strongly correlate with bulk-rock radiogenic
615 isotope composition (Gurenko et al. 2009, 2010) and (c) the diffusion rate of oxygen in
616 olivine is several order of magnitude slower that that of Fe, Mg, Ni, Mn and Ca
617 (Chakraborty 1997; Coogan et al. 2005; Costa and Dungan 2005). In other words, if
618 olivine-melt re-equilibration would have occurred, the grain to grain major and minor
619 element variability would have disappeared first, while the oxygen isotope variability
620 would be still present. The cores of individual olivine phenocrysts, however, are
621 homogeneous in Fo, Ni, Mn and Ca across the grains, except for a thin (20–100 μm)
622 crystal rims just at the contact with groundmass, and show a wide range of Fo, Ni, Mn and
623 Ca in each individual lava sample (Gurenko et al., 2006, 2009, 2010).
624 Because the grain-to-grain major and minor element heterogeneity does exist in
625 each individual lava sample, residence time appears to be insufficient to anneal any cation
626 variability. The times inferred from O, Mg and Fe differ significantly. Tens to a few
627 hundred years are required to erase the observed grain-to-grain 1.4‰ oxygen isotope
628 variability (assigning the size of olivine crystals – from 300 μm to 1 mm – to the distance
629 from planar interface to calculate diffusion rate and $D_{O\text{-}18}$ = 1.1E–16 m^2/s at 1280°C taken
630 from Muehlenbachs and Kushiro 1974) but only 1 day to 1 month is required to account
631 for the observed up to 100 μm rim-to-core Mg-Fe zoning in individual olivine crystals,
632 assuming $D_{Fe\text{-}Mg}$ = 3.9E–11 m^2/s at 1280°C taken from Chakraborty (1997). This implies
633 that the host basalts rapidly carried olivines entrained from crystal cumulates differing in
634 $\delta^{18}O$ values.
635
636 **Acknowledgements** We thank the Ocean Drilling Program for providing AAG with the
637 ODP Leg 157 samples. This work was supported by the CNRS “poste rouge” grant to AG,

638 the NSF EAR-CAREER-0844772 grant to IB and the CRPG-CNRS and at its initial stage
639 by the DFG (grant SCHM 250/64) and the Alexander von Humboldt Foundation
640 (Wolfgang Paul Award to A.V. Sobolev who provided access to the electron microprobe at
641 the Max Planck Institute, Mainz, Germany). C. Harris, A. Schmidt, V. Troll and two
642 anonymous referees provided very insightful reviews and comments to the early
643 manuscript version. This is CRPG contribution number 1924.
644
645

References

Alt JC, Muehlenbachs K, Honnorez J (1986) An oxygen isotopic profile through the upper kilometer of the oceanic crust, DSDP hole 504B. Earth Planet Sci Lett 80: 217–229

Auer S, Bindeman I, Wallace P, Ponomareva V, Portnyagin M (2009) The origin of hydrous, high-δ^{18}O voluminous volcanism: diverse oxygen isotope values and high magmatic water contents within the volcanic record of Klyuchevskoy volcano, Kamchatka, Russia. Contrib Mineral Petrol 157: 209–230

Baertschi P (1976) Absolute ^{18}O content of Standard Mean Ocean Water. Earth Planet Sci Lett 31: 341-344

Bebout GE, Barton MD (1989) Fluid flow and metasomatism in a subduction zone hydrothermal system: Catalina Schist terrane, California. Geology 17: 976–980

Bindeman I (2008) Oxygen isotopes in mantle and crustal magmas as revealed by single crystal analysis. In: Putirka KD, Tepley III FJ (eds) Minerals, Inclusions and Volcanic Processes. Rev Mineral Geochem 69, Mineral Soc Am, Washington DC, pp 445–478

Bindeman IN, Eiler JM, Yogodzinski GM, Tatsumi Y, Stern CR, Grove TL, Portnyagin M, Hoernle K, Danyushevsky LV (2005) Oxygen isotope evidence for slab melting in modern and ancient subduction zones. Earth Planet Sci Lett 235: 480–496

Bindeman IN, Sigmarsson O, Eiler JM (2006) Time constraints on the origin of large volume basalts derived from O-isotope and trace element mineral zoning and U-series disequilibria in the Laki and Grímsvötn volcanic system. Earth Planet Sci Lett 245: 245–259

Bindeman IN, Gurenko AA, Sigmarsson O, Chaussidon M (2008) Oxygen isotope heterogeneity and disequilibria of olivine phenocrysts in large volume basalts from Iceland: evidence for magmatic digestion and erosion of Pleistocene hyaloclastites. Geochim Cosmochim Acta 72: 4397–4420

Chakraborty S (1997) Rates and mechanisms of Fe-Mg interdiffusion in olivine at 980°–1300°C. J Geophys Res 102: 12317–12331

Chaussidon M, Libourel G, Krot AN (2008) Oxygen isotopic constraints on the origin of magnesian chondrules and on the gaseous reservoirs in the early Solar System. Geochim Cosmoch Acta 72: 1924–1938

676 Coogan L, Hain A, Stahl S, Chakraborty S (2005) Experimental determination of the
677 diffusion coefficient for calcium in olivine between 900°C and 1500°C. Geochim
678 Cosmochim Acta 69: 3683–3694
679 Costa F, Chakraborty S (2004) Decadal time gaps between mafic intrusion and silicic
680 eruption obtained from chemical zoning patterns in olivine. Earth Planet Sci Lett 227:
681 517–530
682 Costa F, Dungan M (2005) Short time scales of magmatic assimilation from diffusion
683 modeling of multiple elements in olivine. Geology 33: 837–840
684 Day JMD, Pearson DG, Macpherson CG, Lowry D, Carracedo J-C (2009) Pyroxenite-rich
685 mantle formed by recycled oceanic lithosphere: Oxygen-osmium isotope evidence
686 from Canary Island lavas. Geology 37: 555–558
687 Day JMD, Pearson DG, Macpherson CG, Lowry D, Carracedo JC (2010) Evidence for
688 distinct proportions of subducted oceanic crust and lithosphere in HIMU-type mantle
689 beneath El Hierro and La Palma, Canary Islands. Geochim Cosmochim Acta,
690 doi:10.1016/j.gca.2010.08.021
691 Eggins SM (1992) Petrogenesis of Hawaiian tholeiites: 2, aspects of dynamic melt
692 segregation. Contrib Mineral Petrol 110: 398–410
693 Eiler JM (2001) Oxygen isotope variations in basaltic lavas and upper mantle rocks. In:
694 Valley JW, Cole DR (eds) Stable Isotope Geochemistry. Rev Mineral Geochem 43,
695 Mineral Soc Am, Washington DC, pp 319–364
696 Eiler JM, Farley KA, Valley JW, Hauri E, Craig H, Hart SR, Stolper EM (1997a) Oxygen
697 isotope variations in ocean island basalt phenocrysts. Geochim Cosmochim Acta 61:
698 2281–2293
699 Eiler JM, Graham C, Valley JW (1997b) SIMS analysis of oxygen isotopes: matrix effects
700 in complex minerals and glasses. Chem Geol 138: 221–244
701 Geldmacher J, Hoernle K, van den Bogaard P, Duggen S, Werner R (2005) New $^{40}Ar/^{39}Ar$
702 age and geochemical data from seamounts in the Canary and Madeira volcanic
703 province: Support for the mantle plume hypothesis. Earth Planet Sci Lett 237: 85–101

Gurenko AA, Chaussidon M (1995) Enriched and depleted primitive melts included in olivine from Icelandic tholeiites: origin by continuous melting of a single mantle column. Geochim Cosmochim Acta 59: 2905–2917

Gurenko AA, Hansteen TH, Schmincke H-U (1996) Evolution of parental magmas of Miocene shield basalts of Gran Canaria (Canary Islands): constraints from crystal, melt and fluid inclusions in minerals. Contrib Mineral Petrol 124: 422–435

Gurenko AA, Hansteen TH, Schmincke H-U (1998) Melt, crystal, and fluid inclusions in olivine and clinopyroxene phenocrysts from the submarine shield stage hyaloclastites of Gran Canaria, Sites 953 and 956. In: Weaver PPE, Schmincke H-U, Firth JV, Duffield W (eds) Proc ODP Sci Res Ocean Drilling Program, vol 157. College Station, pp 375–401

Gurenko AA, Chaussidon M, Schmincke H-U (2001) Magma ascent and contamination beneath one intraplate volcano: evidence from S and O isotopes in glass inclusions and their host clinopyroxenes from Miocene basaltic hyaloclastites southwest of Gran Canaria (Canary Islands). Geochim Cosmochim Acta 65: 4359–4374

Gurenko AA, Hoernle KA, Hauff F, Schmincke H-U, Han D, Miura YN, Kaneoka I (2006) Major, trace element and Nd-Sr-Pb-O-He-Ar isotope signatures of shield stage lavas from the central and western Canary Islands: Insights into mantle and crustal processes. Chem Geol 233: 75–112

Gurenko AA, Sobolev AV, Hoernle K, Hauff F, Schmincke H-U (2009) Enriched, HIMU-type peridotite and depleted recycled pyroxenite in the Canary plume: a mixed-up mantle. Earth Planet Sci Lett 277: 514–524

Gurenko AA, Hoernle K, Sobolev AV, Hauff F, Schmincke H-U (2010) Source components of the Gran Canaria (Canary Islands) shield stage magmas: evidence from olivine composition and Sr-Nd-Pb isotopes. Contrib Mineral Petrol 159: 689–702

Hansteen TH, Troll VR (2003) Oxygen isotope composition of xenoliths from the oceanic crust and volcanic edifice beneath Gran Canaria (Canary Islands): consequences for crustal contamination of ascending magmas. Chem Geol 193: 181–193

Hoernle K (1998) Geochemistry of Jurassic oceanic crust beneath Gran Canaria (Canary Islands): implications for crustal recycling and assimilation. J Petrol 39: 859–880

734 Hoernle K, Tilton GR (1991) Sr-Nd-Pb isotope data for Fuerteventura (Canary Islands)
735 basal complex and subaerial volcanics: application to magma genesis and evolution.
736 Schweiz Min Petrol Mitt 71: 5–21
737 Hoernle K, Tilton G, Schmincke H-U (1991) Sr-Nd-Pb isotopic evolution of Gran Canaria:
738 evidence for shallow enriched mantle beneath the Canary Islands. Earth Planet Sci
739 Lett 106: 44–63
740 Hoernle K, Zhang Y-S, Graham D (1995) Seismic and geochemical evidence for large-
741 scale mantle upwelling beneath the eastern Atlantic and western and central Europe.
742 Nature 374: 34–39
743 Hofmann AW (1997) Mantle geochemistry: the message from oceanic volcanism. Nature
744 385: 219-229
745 Hofmann AW, White WM (1982) Mantle plumes from ancient oceanic crust. Earth Planet
746 Sci Lett 57: 421–436
747 Kita NT, Ushikubo T, Fu B, Valley JW (2009) High precision SIMS oxygen isotope
748 analysis and the effect of sample topography. Chem Geol 264: 43–57
749 Longpré M-A, Troll VR, Hansteen TH (2008) Upper mantle magma storage and transport
750 under a Canarian shield-volcano, Teno, Tenerife (Spain). J Geophys Res 113: B08203,
751 doi:10.1029/2007JB005422
752 Lundstrom CC, Hoernle K, Gill J (2003) U-series disequilibria in volcanic rocks from the
753 Canary Islands: Plume versus lithospheric melting. Geochim Cosmochim Acta 67:
754 4153–4177
755 Marcantonio F, Zindler A, Elliott T, Staudigel H (1995) Os isotope systematics of La
756 Palma, Canary Islands; evidence for recycled crust in the mantle source of HIMU
757 ocean islands. Earth Planet Sci Lett 133: 397–410
758 Mattey D, Lowry D, Macpherson C (1994) Oxygen isotope composition of mantle
759 peridotite. Earth Planet Sci Lett 128: 231–241
760 McKenzie D (1985) The extraction of magma from the crust and mantle. Earth Planet Sci
761 Lett 74: 81–91
762 Mojzsis SJ, Harrison TM, Pidgeon RT (2001) Oxygen-isotope evidence from ancient
763 zircons for liquid water at the Earth's surface 4,300 Myr ago. Nature 409: 178–181

764 Montelli R, Nolet G, Dahlen FA, Masters G, Engdahl ER, Hung S-H (2004) Finite-
765 frequency tomography reveals a variety of plumes in the mantle. Science 303:
766 338–343
767 Muehlenbachs K (1986) Alteration of the oceanic crust and the ^{18}O history of seawater. In:
768 Valley JW, Taylor Jr, HP, O'Neil JR (eds) Stable Isotopes in High Temperature
769 Geological Processes. Rev Mineral, vol 16. Mineral Soc Am, Washington DC, pp
770 425–444
771 Muehlenbachs K, Kushiro I (1974) Oxygen isotopic exchange and equilibrium of silicates
772 with CO_2 and O_2. Carnegie Inst Wash Yearbook 73: 232–236
773 Putlitz B, Matthews A, Valley JW (2000) Oxygen and hydrogen isotope study of high-
774 pressure metagabbros and metabasalts (Cyclades, Greece): Implications for the
775 subduction of oceanic crust. Contrib Mineral Petrol 138: 114–126
776 Shaw DM (1970) Trace element fractionation during anatexis. Geochim Cosmochim Acta
777 34: 237–243
778 Simonsen SL, Neumann E-R, Seim K (2000) Sr-Nd-Pb isotope and trace-element
779 geochemistry evidence for a young HIMU source and assimilation at Tenerife (Canary
780 Island). J Volcanol Geotherm Res 103: 299–312
781 Sobolev AV, Shimizu N (1993) Ultra-depleted primary melt included in an olivine from
782 the Mid-Atlantic Ridge. Nature 363: 151–154
783 Sobolev AV, Hofmann AW, Nikogosian IK (2000) Recycled oceanic crust observed in
784 "ghost plagioclase" within the source of Mauna Loa lavas. Nature 404: 986–990
785 Sobolev AV, Hofmann AW, Sobolev SV, Nikogosian IK (2005) An olivine-free mantle
786 source of Hawaiian shield basalts. Nature 434: 590–597
787 Sobolev AV, Hofmann AW, Kuzmin DV, Yaxley GM, Arndt NT, Chung S-L,
788 Danyushevsky LV, Elliott T, Frey FA, Garcia MO, Gurenko AA, Kamenetsky VS,
789 Kerr AC, Krivolutskaya NA, Matvienkov VV, Nikogosian IK, Rocholl A, Sigurdsson
790 IA, Sushchevskaya NM, Teklay M (2007) The amount of recycled crust in sources of
791 mantle-derived melts. Science 316: 412–417
792 Sobolev AV, Hofmann AW, Brügmann B, Batanova VG, Kuzmin DV (2008) A
793 quantitative link between recycling and osmium isotopes. Science 321: 536
794 Taylor JR (1982) An introduction to error analysis. Oxford Univ Press, Oxford

795 Taylor Jr HP, Sheppard SMF (1986) Igneous rocks: I. Processes of isotopic fractionation
796 and isotopic systematics. In: Valley JW, Taylor Jr HP, O'Neil JR (eds) Stable Isotopes
797 in High Temperature Geological Processes. Rev Mineral, vol 16. Mineral Soc Am,
798 Washington DC, pp 227–271
799 Thirlwall MF, Jenkins C, Vroon PZ, Mattey DP (1997) Crustal interaction during
800 construction of oceanic islands: Pb-Sr-Nd-O isotope geochemistry of the shield basalts
801 of Gran Canaria, Canary Islands. Chem Geol 135: 233–262
802 Turner S, Tonarini S, Bindeman I, Leeman WP, Schaefer BF (2007) Boron and oxygen
803 isotope evidence for recycling of subducted components over the past 2.5 Gyr. Nature
804 447: 702–705
805 Valley JW, Graham CM (1991) Ion microprobe analysis of oxygen isotope ratios in
806 granulite facies magnetites: diffusive exchange as a guide to cooling history. Contrib
807 Mineral Petrol 109: 38–52
808 Valley JW, Kitchen N, Kohn MJ, Niendorf CR, Spicuzza MJ (1995) UWG-2, a garnet
809 standard for oxygene isotope ratios: Strategies for high precision and accuracy with
810 laser heating. Geochim Cosmochim Acta 59: 5223–5231
811 van der Hilst R, Engdahl R, Spakman W, Nolet G (1991) Tomographic imaging of
812 subducted lithosphere below northwest pacific island arcs. Nature 353: 37–43
813 van der Hilst R, Widiyantoro RS, Engdahl R (1997) Evidence for deep mantle circulation
814 from global tomography. Nature 386: 578–584
815 Walter MJ (1998) Melting of garnet peridotite and the origin of komatiite and depleted
816 lithosphere. J Petrol 39: 29–60
817 Wang Z, Eiler JM (2008) Insights into the origin of low-$\delta^{18}O$ basaltic magmas in Hawaii
818 revealed from in situ measurements of oxygen isotope compositions of olivines. Earth
819 Planet Sci Lett 269: 376–386
820 Widom E, Farquhar J (2003) Oxygen isotope signatures in olivines from Sao Miguel
821 (Azores) basalts: implications for crustal and mantle processes. Chem Geol 193:
822 237–255
823 Widom E, Hoernle KA, Shirey SB, Schmincke H-U (1999) Os isotope systematics in the
824 Canary Islands and Madeira: Lithospheric contamination and mantle plume signatures.
825 J Petrol 40: 297–314

826 Williams RW, Gill JB (1989) Effects of partial melting on the uranium decay series.
827 Geochim Cosmochim Acta 53: 1607–1619
828 Yaxley G, Sobolev A (2007) High-pressure partial melting of gabbro and its role in the
829 Hawaiian magma source. C1ontrib Mineral Petrol 154: 371–383
830 Zeb Page FZ, Ushikubo T, Kita NT, Riciputi LR, Valley JW (2007) High-precision oxygen
831 isotope analysis of picogram samples reveals 2 μm gradients and slow diffusion in
832 zircon. Am Miner 92: 1772–1775
833 Zindler A, Hart S (1986) Chemical geodynamics. Ann Rev Earth Planet Sci 14: 493–571
834
835

836 **Figure captions**

837 Fig. 1. The position of the Canary Islands relative to the western coast of Africa (modified
838 after Lundstrom et al. 2003). The numbers in parenthesis below the island/seamount names
839 refer to the oldest ages in million years obtained for shield stage volcanism from these
840 islands/seamounts (see Geldmacher et al. 2005), indicating a crude SW to NE progression
841 of increasing age. The circle to the NE of Gran Canaria labeled by "953" represents a
842 position of Site 953 drilled during the ODP Leg 157.

843

844 Fig. 2. Composition of the Canarian olivines analyzed for O isotopes; (A) NiO and (B)
845 MnO concentrations vs. forsterite (Fo) contents, (C) Ni×FeO/MgO vs. Mn/FeO ratios.
846 *SCO* = San Carlos olivine USNM 111312/444 analyzed as unknown together with samples
847 of interest and representing real analytical uncertainty of EPMA.

848

849 Fig. 3. Instrumental mass fractionation (*IMF*) obtained during secondary ion mass
850 spectrometry (*SIMS*) analyses (A) and correspondence of SIMS and laser fluorination (*LF*)
851 methods (B). (A) IMF (given in ‰) measured on SCO ($Fo_{90.7}$) vs. IMF on CI114 ($Fo_{74.2}$)
852 reference olivines, demonstrating no relation of IMF as a function of olivine chemical
853 composition. (B) $\delta^{18}O_{olivine}$ values obtained by SIMS and LF methods for the same olivine
854 crystals. Error bars represent average $\pm 2\sigma$ analytical uncertainty of a single measurement
855 by SIMS (±0.34‰ during this study and ±0.5‰ obtained by Bindeman et al. 2008) versus
856 that of LF (±0.18‰).

857

858 Fig. 4. Oxygen isotopic composition of individual olivine grains analyzed by SIMS and LF
859 methods. The shaded vertical band marks the range of typical upper mantle olivine
860 (4.8–5.4‰; Mattey et al. 1994) and of olivine in equilibrium with N-MORB magmas
861 (assuming olivine-melt fractionation of −0.4‰ and the N-MORB range of 5.2–5.9‰, Eiler
862 et al. 2000). We point out the good agreement between SIMS and LF results. Error bars
863 represent average $\pm 2\sigma$ analytical uncertainty of each method. In this figure and Figs. 5
864 through 7, the $\delta^{18}O$ values are given in permil units and defined relative to the Standard

865 Mean Ocean Water (SMOW, $^{18}O/^{16}O$ = 0.0020052 ± 0.00000043; Baertschi 1976)
866 standard i.e., $\delta^{18}O = [(^{18}O/^{16}O_{sample} - {}^{18}O/^{16}O_{SMOW}) / {}^{18}O/^{16}O_{SMOW}] \times 1000$, ‰].
867
868 Fig. 5. Relationships between $\delta^{18}O$ values of individual olivine phenocrysts vs. their Fo
869 contents (A-C) and Ni×FeO/MgO ratios (D-F). Panels (A, B, D, E) represent olivine
870 composition analyzed by SIMS from the western (A, D) and eastern (B, E) Canary Islands;
871 panels (C, F) represent olivine compositions analyzed by LF. The $\delta^{18}O_{olivine}$ values show
872 significant scatter, either obtained by SIMS or by LF. Subtle correlations of $\delta^{18}O_{olivine}$
873 values with Fo (R^2 = 0.36) and Ni×FeO/MgO ratios (R^2 = 0.29) were found for one El
874 Hierro sample. *Contamination* trend shown in panels (A-C) demonstrates possible coherent
875 decrease of Fo and $\delta^{18}O_{olivine}$ values due to magma contamination at shallow depth, found
876 in the Mauna Loa and Mauna Kea subaerial lavas by Wang and Eiler (2008). The error
877 bars represent average $\pm 2\sigma$ analytical uncertainty of SIMS and LF methods.
878
879 Fig. 6. The relationship between $\delta^{18}O_{olivine}$ and Ni×FeO/MgO ratios of individual olivine
880 phenocrysts from EH4 basanite (El Hierro). The error bars represent $\pm 2\sigma$ analytical
881 uncertainty. The uncertainties of $\delta^{18}O_{olivine}$ values of the peridotite and pyroxenite
882 endmembers were calculated assuming two sources of independent random errors: (1) the
883 analytical uncertainty of individual measurements and (2) the uncertainty caused by
884 deviations of the measured $\delta^{18}O_{olivine}$ values from the regression line (Taylor 1982).
885
886 Fig. 7. The effects of different source lithology on the oxygen isotope composition of the
887 peridotite and pyroxenite derived partial melts. The $\delta^{18}O$ values given as a function of
888 partial melting degree were calculated assuming initial $\delta^{18}O_{init}$ = 4.8‰ for peridotite i.e.
889 the "olivine equivalent" obtained for the El Hierro peridotite source (**Fig. 6**) and varying
890 $\delta^{18}O_{init}$ values (4.6‰, 4.8‰ and 6.1‰, respectively) for pyroxenite (see text). The oxygen
891 isotope equilibrium fractionation factors between minerals (olivine, orthopyroxene,
892 clinopyroxene, garnet and quartz) and picrite melt at 1400°C are taken from Eiler (2001)
893 and listed in **Table 1**. The phase proportions and partial melting degrees were taken

894 directly from experiments of Walter (1998) for garnet peridotite and Yaxley and Sobolev
895 (2007) and Sobolev et al. (2007) for pyroxenite (**Table 1**). The shaded *hybrid melt* fields
896 outline oxygen isotope compositions of the probable hybrid magmas originated after
897 mixing of pure peridotite and pyroxenite partial melts taking into account partial melting
898 degrees of coexisting peridotite and pyroxenite at given P-T conditions (i.e.,
899 $F_{peridotite}$:$F_{pyroxenite}$ = 4:25, 6:35 and 11:41; **Table 1** in Sobolev et al. 2005). We emphasize
900 that oxygen isotope fractionation during partial melting of peridotite and pyroxenite mantle
901 sources having the same oxygen isotope composition (i.e., $\delta^{18}O$ = 4.8‰) but differing
902 significantly in the proportions of rock-forming mineral phases causes only less than 0.2‰
903 in the resulting partial melts.

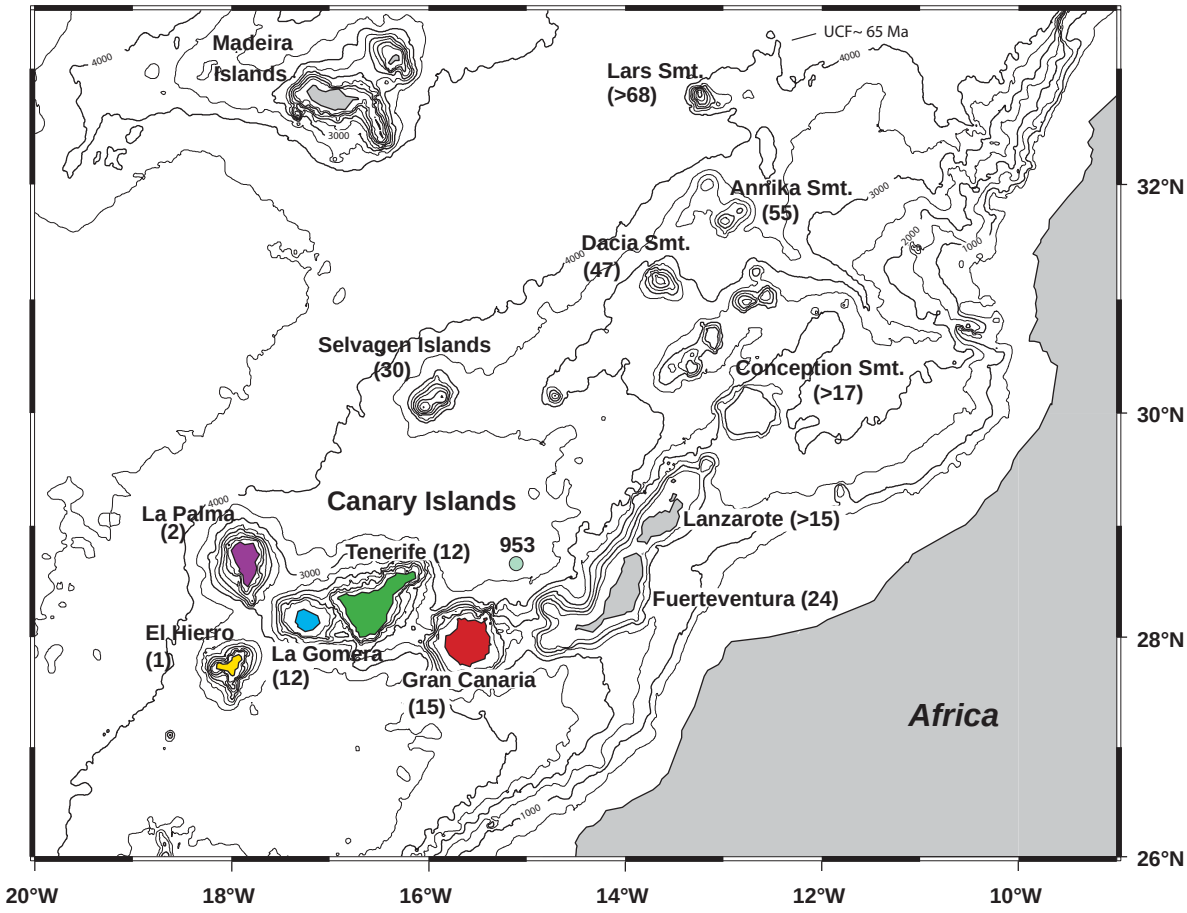

Fig. 1: Gurenko et al.

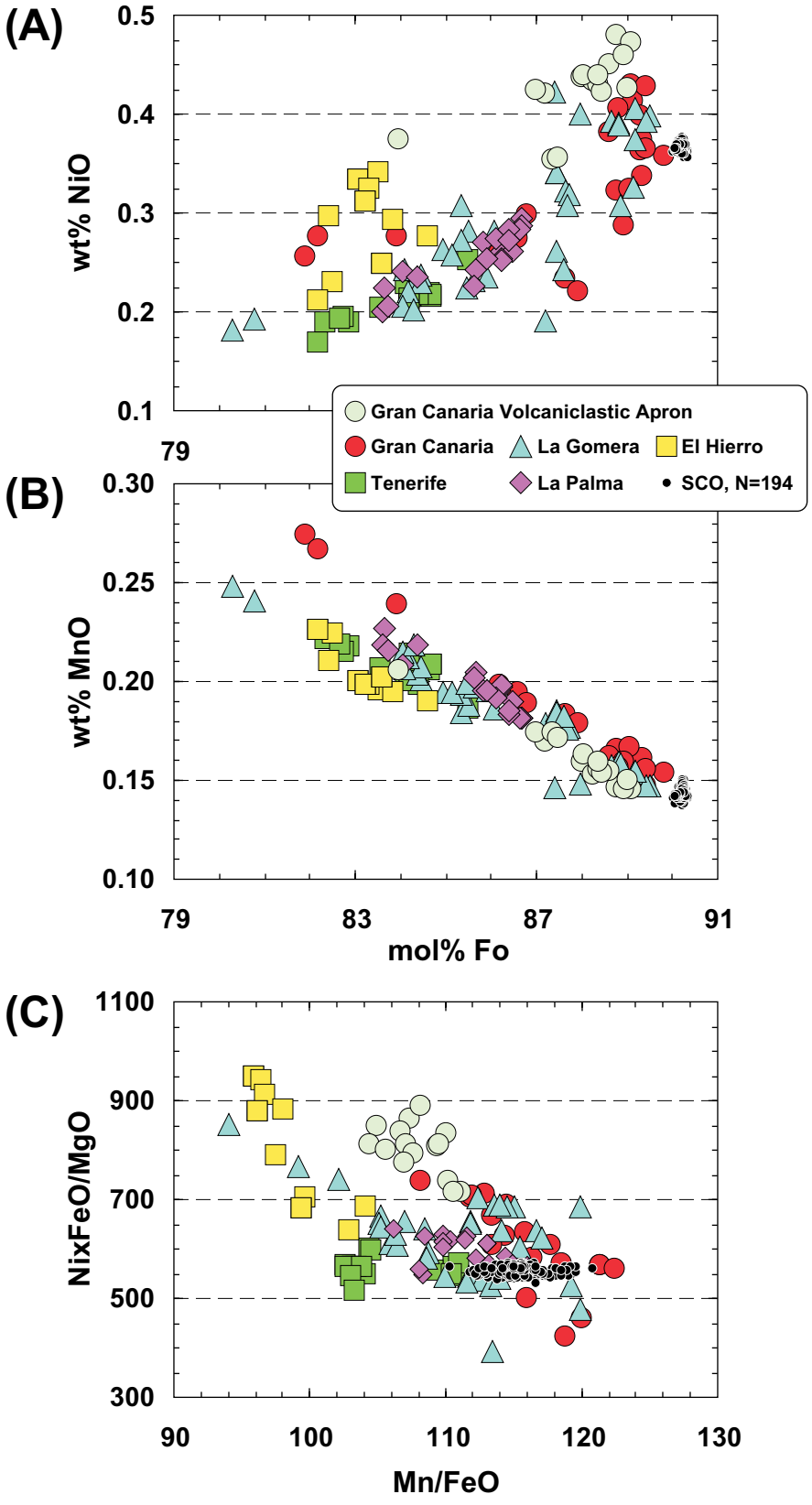

Fig. 2. Gurenko et al.

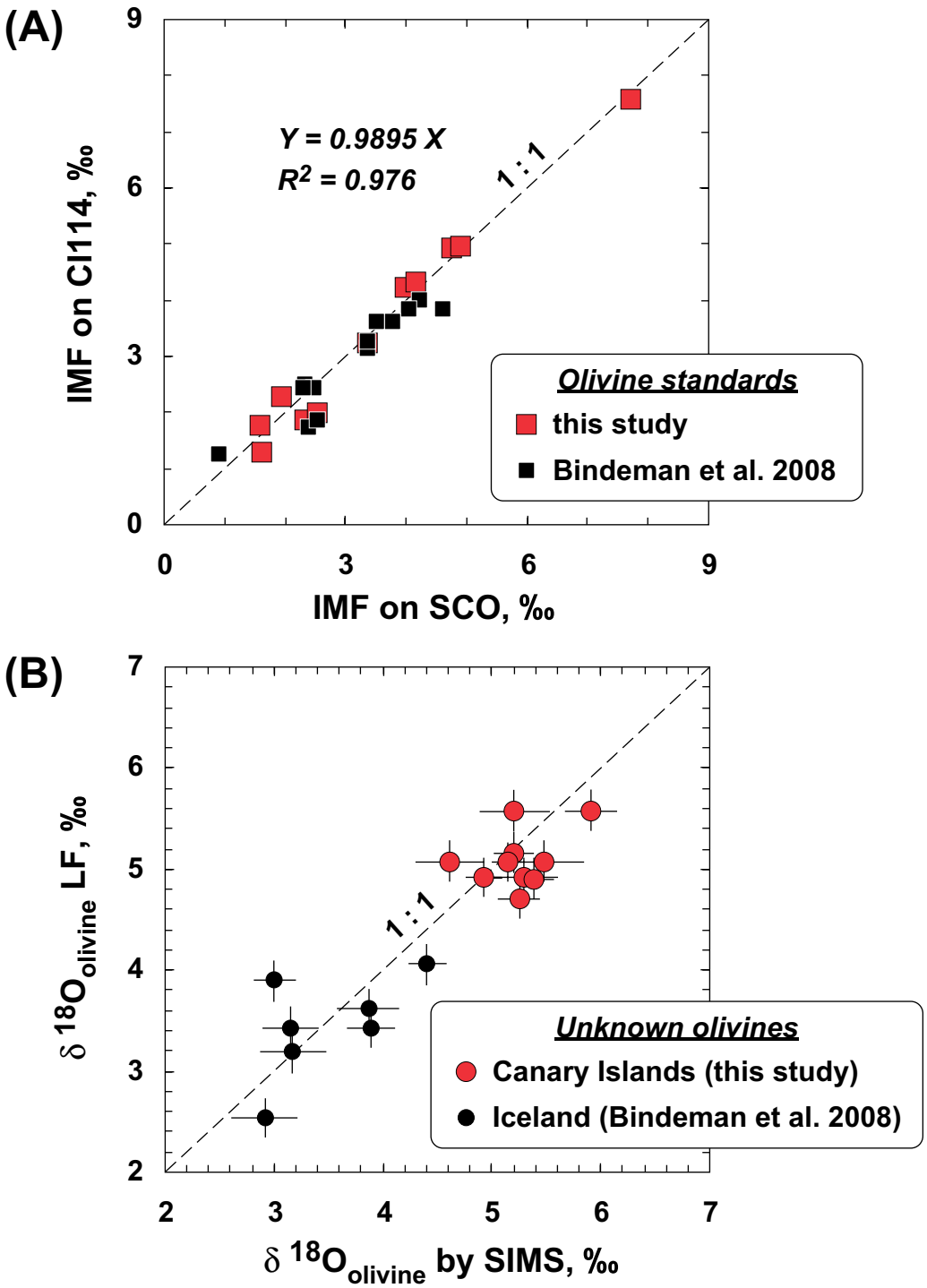

Fig. 3. Gurenko et al.

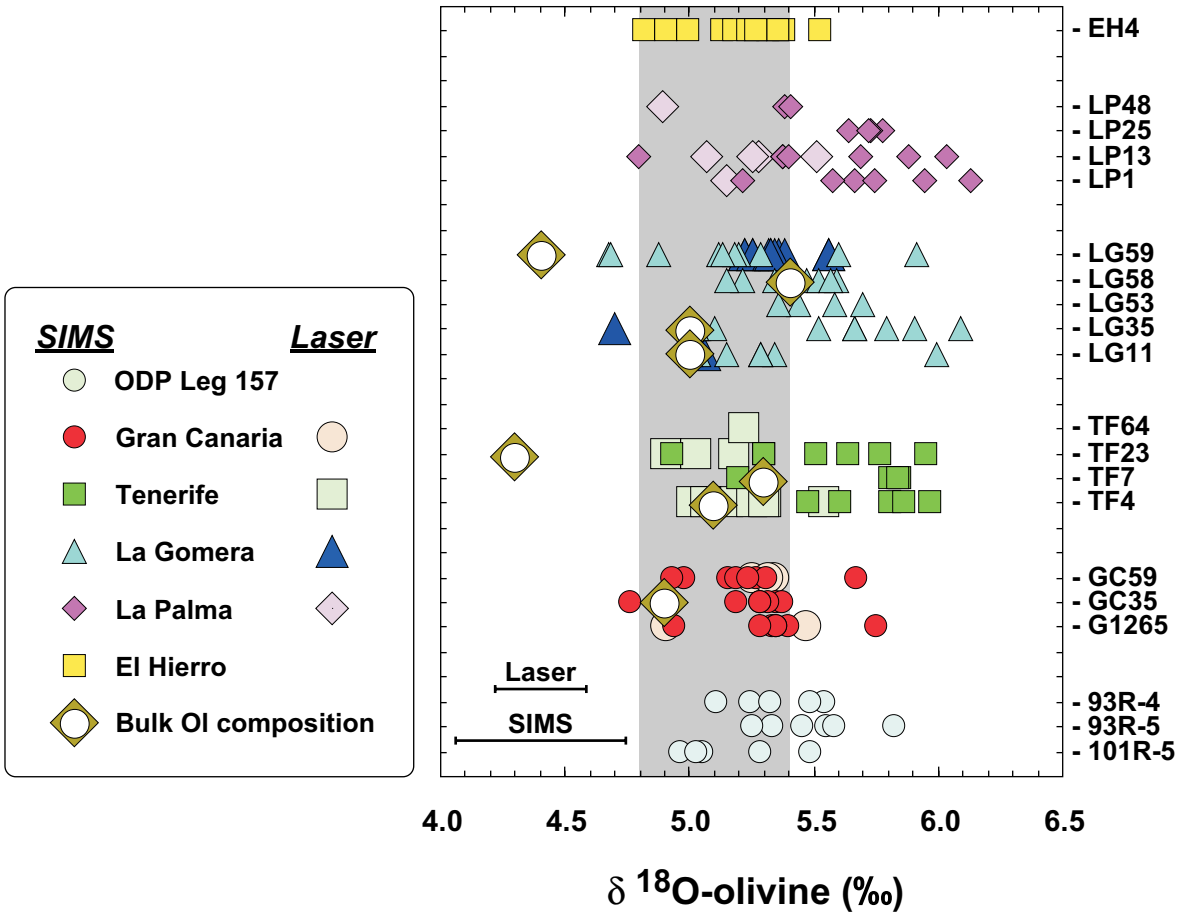

Fig. 4. Gurenko et al.

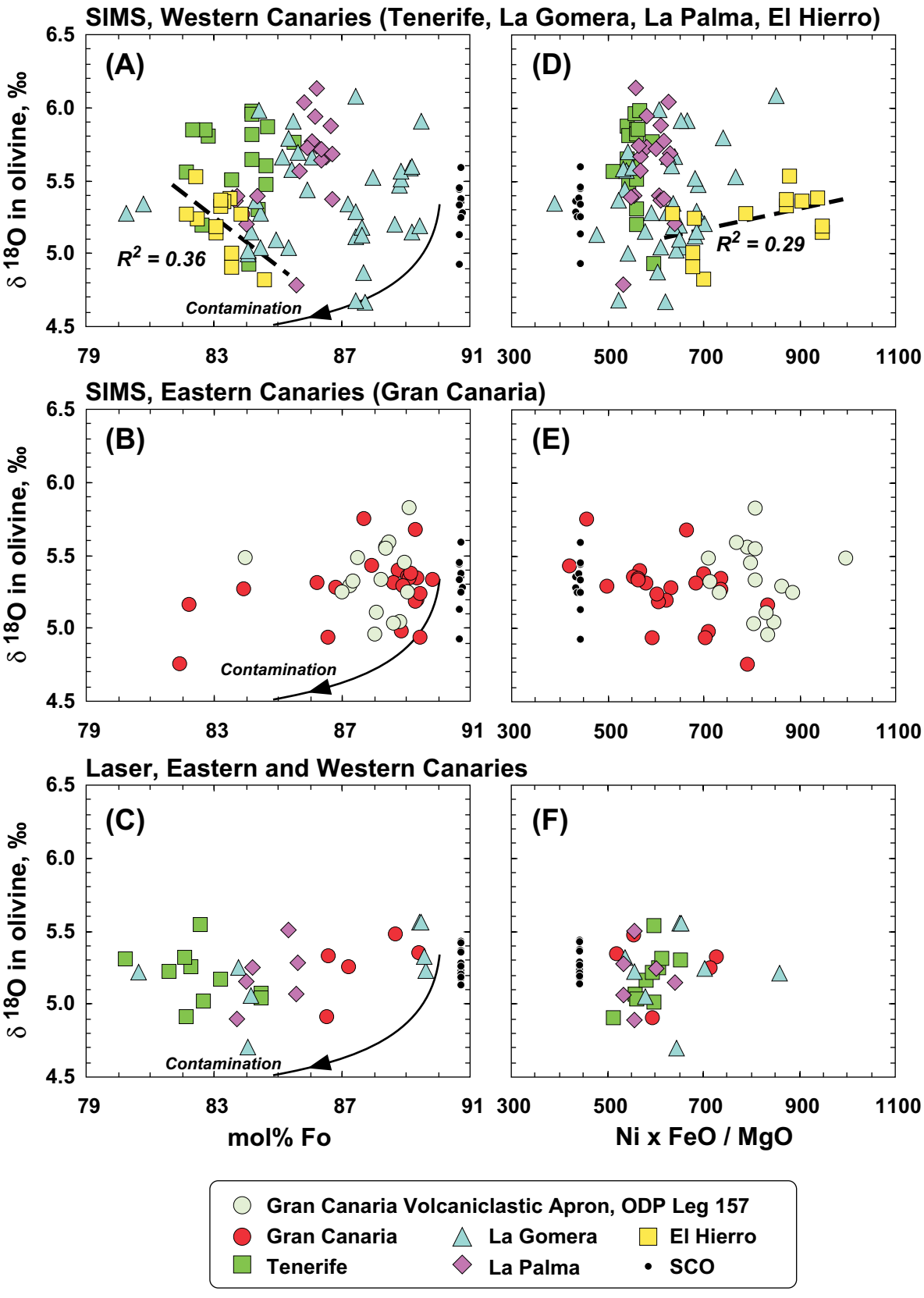

Fig. 5. Gurenko et al.

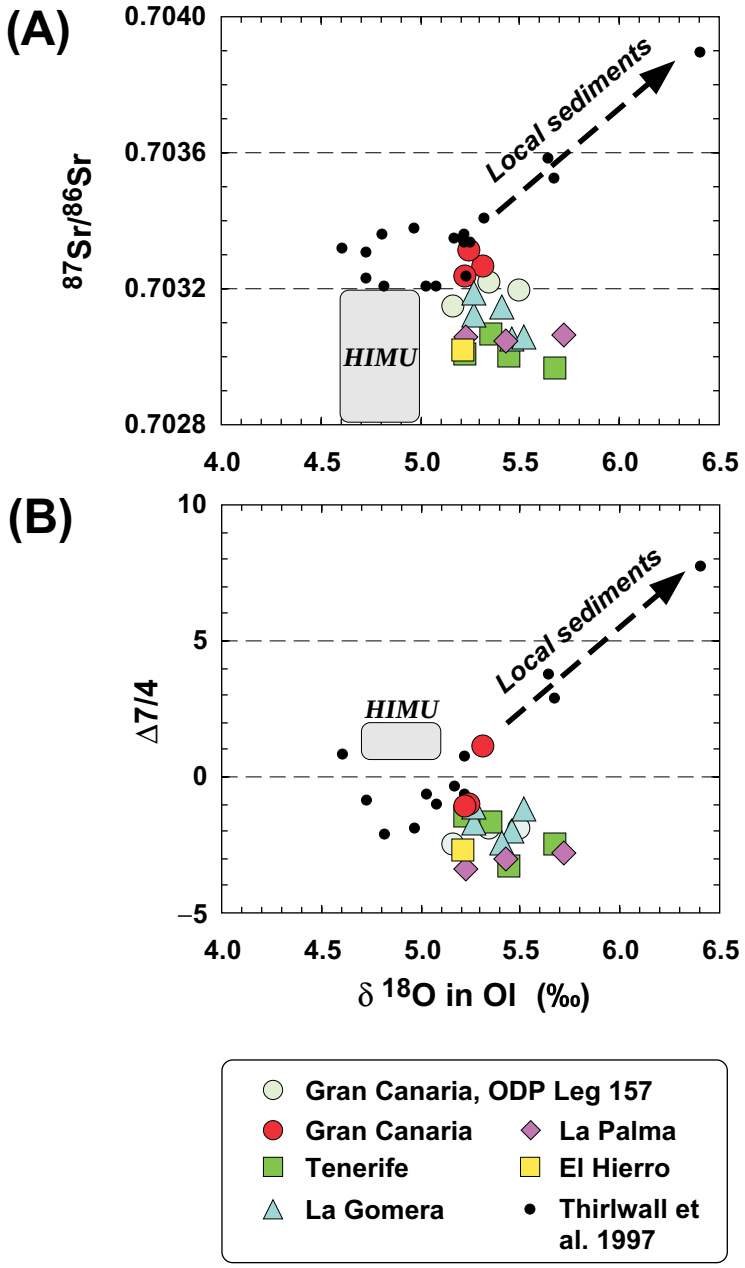

Fig. 6. Gurenko et al.

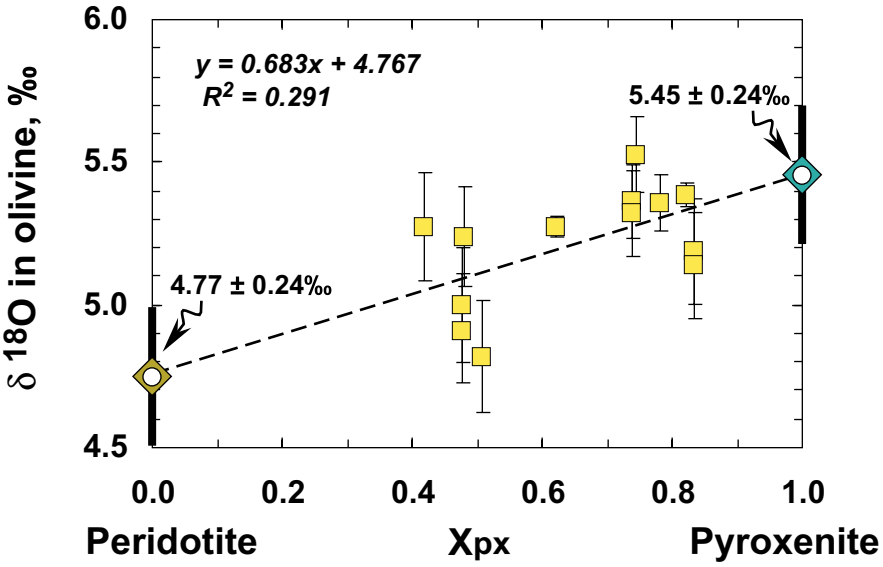

Fig. 7. Gurenko et al.

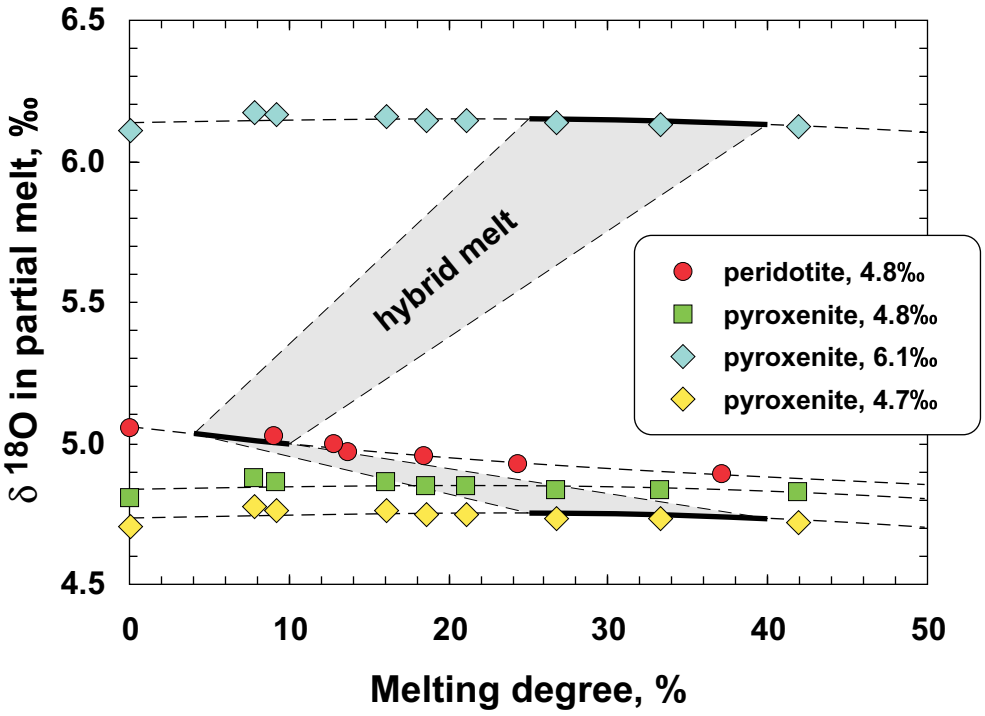

Fig. 8. Gurenko et al.